Analyst

PAPER

View Article Online
View Journal | View Issue

Cite this: *Analyst*, 2016, **141**, 6104

Fiber enhanced Raman spectroscopic analysis as a novel method for diagnosis and monitoring of diseases related to hyperbilirubinemia and hyperbiliverdinemia†

Di Yan,[a] Christian Domes,[a] Robert Domes,[a] Timea Frosch,[a] Jürgen Popp,[a,c,d] Mathias W. Pletz[b] and Torsten Frosch*[a,c,d]

Fiber enhanced resonance Raman spectroscopy (FERS) is introduced for chemically selective and ultrasensitive analysis of the biomolecules hematin, hemoglobin, biliverdin, and bilirubin. The abilities for analyzing whole intact, oxygenated erythrocytes are proven, demonstrating the potential for the diagnosis of red blood cell related diseases, such as different types of anemia and hemolytic disorders. The optical fiber enables an efficient light-guiding within a miniaturized sample volume of only a few micro-liters and provides a tremendously improved analytical sensitivity (LODs of 0.5 μM for bilirubin and 0.13 μM for biliverdin with proposed improvements down to the pico-molar range). FERS is a less invasive method than the standard ones and could be a new analytical method for monitoring neonatal jaundice, allowing a precise control of the unconjugated serum bilirubin levels, and therefore, providing a better prognosis for newborns. The potential for sensing very low concentrations of the bile pigments may also open up new opportunities for cancer research. The abilities of FERS as a diagnostic tool are explored for the elucidation of jaundice with different etiologies including the rare, not yet well understood diseases manifested in green jaundice. This is demonstrated by quantifying clinically relevant concentrations of bilirubin and biliverdin simultaneously in the micro-molar range: for the case of hyperbilirubinemia due to malignancy, infectious hepatitis, cirrhosis or stenosis of the common bile duct (1 μM biliverdin together with 50 μM bilirubin) and for hyperbiliverdinemia (25 μM biliverdin and 75 μM bilirubin). FERS has high potential as an ultrasensitive analytical technique for a wide range of biomolecules and in various life-science applications.

Received 23rd July 2016,
Accepted 20th August 2016

DOI: 10.1039/c6an01670g

www.rsc.org/analyst

Introduction

Heme chromophores are iron protoporphyrin IX complexes and fulfil essential roles in several regulating processes in biological systems. They serve for instance as catalytically active centers of different important cytochrome enzymes, which have important functions in biochemical processes, among others in the brain,[1] and represent the prosthetic group of hemoglobin, the transporter of respiratory gases (O_2, CO_2, CO) in erythrocytes.[2] Therefore, monitoring of the oxygenation state of the red blood cells can be very helpful for the differential diagnosis of different types of anemia and hemolytic disorders. Heme and hemozoin are also key drug-targets in blood disorders and diseases, such as malaria.[3] In the blood recycling process, the aged red blood cells are degraded into their components, heme and globin. The heme group is enzymatically converted to biliverdin (BV) and bilirubin (BR),[4] which can be eliminated *via* bile after biotransformation (conjugation) in the liver (Fig. 1). When the activity of one of the participating enzymes is defect or totally absent, this detoxification process is perturbed and several diseases might occur.[5]

An increased level of bilirubin above normal, so called hyperbilirubinemia, is shown to be toxic and in most cases manifests in jaundice,[6] a yellow tint of the skin and sclera. The toxicity of hyperbilirubinemia is especially important in neonates due to incomplete formation of the blood–brain barrier,[7] in which case the circulating unconjugated excess bilirubin may pose a threat to the infant by entering the central nervous system and thereby causing irreversible neurological damage by developing kernicterus or bilirubin-encephalopathy.[8] About 60% of healthy, term neonates present detectable jaundice[9]

[a]*Leibniz Institute of Photonic Technology, Jena, Germany*
[b]*University Hospital, Center for Infectious Diseases and Infection Control, Jena, Germany*
[c]*Friedrich Schiller University, Institute for Physical Chemistry, Jena, Germany*
[d]*Friedrich Schiller University, Abbe Centre of Photonics, Jena, Germany.*
E-mail: torsten.frosch@uni-jena.de, torsten.frosch@gmx.de

†Electronic supplementary information (ESI) available. See DOI: 10.1039/c6an01670g

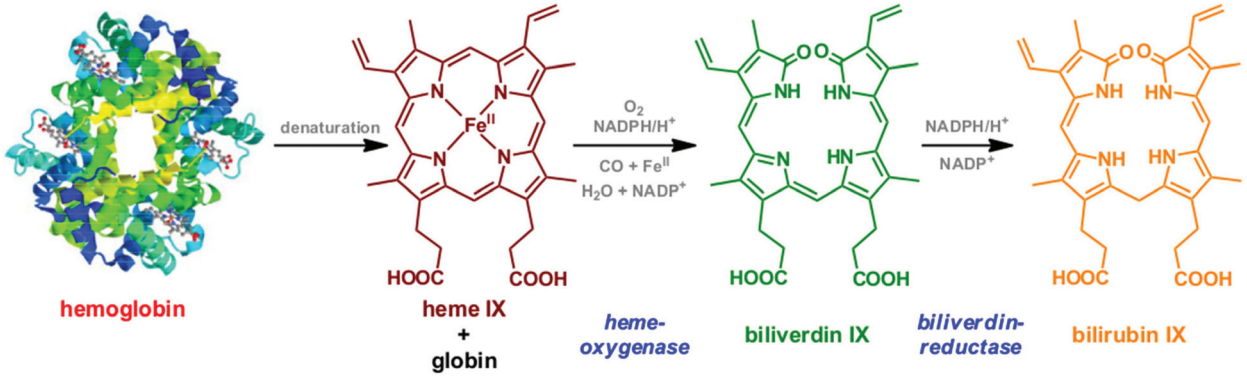

Fig. 1 Scheme of the metabolism of hemoglobin by various enzymes. The first step is the denaturation of hemoglobin tetramer by phagocytes to heme IX and globin chains. In the reticular connective tissue, the heme chromophore is enzymatically oxidized by *heme oxygenase* in presence of oxygen to the green bile pigment biliverdin IX. Due to the effect of the enzyme *biliverdin reductase* this pigment is reduced to its orange degradation product, bilirubin IX.

and even low elevations of the bilirubin level can manifest in an increased incidence of neurological abnormalities or decreased development of intellectual performance later in life.[10] Early discharged babies may only present jaundice at extremely high serum bilirubin concentrations.[11]

For ensuring a better prognosis, an earlier diagnosis of mild hyperbilirubinemia is needed, before the manifestation of jaundice. Thus, an extremely sensitive method is required for rapid monitoring of the serum bilirubin level. This technique should also be minimally invasive and require only minimal blood sample volume for quantification.

Moreover, an elevation of the bilirubin serum level from 17 μM up to 340 μM (ref. 10) was also observed in the inheritable disorders Gilbert[5c] and Crigler–Najjar syndrome.[5d] Therefore, the detection of these elevations could be very helpful as an early diagnostic indicator before genetical investigations.

Hyperbiliverdinemia, defined as elevated level of biliverdin above the normal range, is another type of jaundice, so called green jaundice.[12] Normal biliverdin levels in serum are reported as 0.9–6.5 μM and strongly correlate to the total bilirubin concentration,[13] whereas green jaundice manifests in a rise of the serum level of bilirubin above 25 μM together with an elevation of biliverdin level above 75 μM.[13] This symptom occurs in several syndromes and diseases.[13,14] The serum biliverdin concentration is found by patients diagnosed with malignancy, infectious hepatitis, cirrhosis or stenosis of the common bile duct jaundice to be in the range from one to ten percentage of the total bilirubin level.[14b] On the other hand, the absence of hyperbiliverdinemia is an indication against the diagnosis of jaundice due to neoplastic obstruction.[12] Thus, being able to simultaneously quantify slight elevations of bilirubin and biliverdin levels would be tremendously helpful for the diagnosis of the cause of jaundice.

Additionally, in the past two decades, medical scientists have discovered beneficial properties of the bile pigments. They play an important role as anti-oxidative[15] and anti-mutagenic agents[16] at slightly elevated biliverdin level of 15 μM.[16b] Also an HIV-protease inhibiting activity above the concentration of 10 μM is assigned to the bile pigments.[17] At the concentration of 25 μM, bilirubin induces apoptosis significantly in human gastric adenocarcinoma cell lines[18] and also in colon cancer cells.[19] The presence of 15 μM biliverdin successfully inhibits the mutations in mammalian cell systems.[20] These beneficial properties of the bile pigments are also reflected in clinical studies. An increase of the bilirubin level by 1.7 μM is correlated with 8% reduction of the incidence rate of lung cancer and with 6% reduction of the rate of chronic obstructive pulmonary disease.[15a]

Therefore, the simultaneous detection of minor concentration changes (micro-molar and lower concentrations) of biliverdin and bilirubin is urgently needed for the earlier diagnosis and monitoring of diseases, such as malignancy, infectious hepatitis, cirrhosis, and stenosis of the common bile duct jaundice as well as for neonatal jaundice, and also for the elucidation of important processes in cancer research.

Several methods have been developed for the analysis of bilirubin in clinical samples. The most commonly used ones are the diazo reaction[21] and the direct spectrophotometry.[22] These techniques are highly dependent on the pH-value or have interference with other heme containing proteins, and both are very time-consuming. Therefore, there is a need of extremely sensitive method for rapid monitoring the serum bilirubin level. In the last few decades the trend goes to other analytical methods like photochemical[23] or electrochemical sensors[24] and chromatography[25] which are used for the detection of bilirubin in human serum. Since there are no investigations of the biliverdin and bilirubin level in terms of the analysis of jaundice and other diseases *via* fiber enhanced Raman spectroscopy (FERS), this paper should demonstrate the potential of this technique as a tool for sensitive and chemical selective analysis of these two bile pigments together in clinically relevant concentrations. The advantage here is the minimally invasiveness and the need of minimal sample volumes for their simultaneous quantification. None of the other methods incorporate these characteristics altogether. In

fiber enhanced Raman spectroscopy, the signal intensity is significantly increased by exciting and collecting the Raman signal of the liquid sample along an extended path length within the fiber hollow core with remarkable efficiency. Excellent results have been achieved in the analysis of low concentrated analytes in aqueous solutions.[26]

Materials and methods

Sample preparation

Hemin (chloroferriprotoporphyrin IX, ≥98.0%), human lyophilized hemoglobin, bilirubin (95%), biliverdin-hydrochloride (97%), and phosphate buffered saline were purchased from Sigma-Aldrich and used without further purification (Fig. 2). An ultra-clear water feed system from SG Water GmbH was employed to produce ultrapure deionized water (conductivity lower than 0.056 μS cm^{-1}). Hematin solutions (pH 7) were prepared by dissolving hemin in 0.1 M NaOH and then diluted with deionized water to various concentrations. Hemoglobin, bilirubin and biliverdin were buffered at pH 7.4 in all concentrations. Erythrocytes were separated from human blood. The human blood was centrifuged at 3000 rpm for 10 min. Then the upper part of the solution was removed from the tube, and phosphate buffered saline (PBS: 10 mM PO_4^{3-}, 137 mM NaCl, 1.8 mM KH_2PO_4, and 2.7 mM KCl) was refilled into the tube. This procedure was repeated three times. Then the erythrocytes were diluted 1 : 199 with PBS (pH 7.4). All samples were kept in the dark at 4 °C until use.

Fiber enhanced Raman spectroscopy

Raman spectra were obtained with a LabRam HR system with excitation wavelengths λ = 532 nm (I_{laser} = 10 mW at the sample), λ = 413 nm (I_{laser} = 7 mW at the sample), λ = 752 nm (I_{laser} = 350 mW at the sample) and λ = 364 nm (I_{laser} = 3.5 mW at the sample). A 10× objective lens (Olympus) and a 15× objective lens (OFR) were used for the measurements in the visible and UV ranges, respectively. The optical hollow core fiber had a length of 40 cm, an inner diameter of 168 μm and an internal volume of 9 μL. In order to keep a stable optical coupling situation for quantitative and reproducible Raman sensing, a custom-made fiber adapter which provides an optical window for laser coupling into the fiber was also developed[27] (Fig. 3). In order to avoid photo-degradation of the absorbing analytes during the measurements, the samples were kept streaming at 40 μL s^{-1} flow rate with the help of a syringe pump. Thus, the velocity of liquids in the fiber was about 1.8 m s^{-1} and the samples passed through the laser focus within a short time and were not damaged by the laser radiation. All spectra were taken with 120 s exposure time, and the performance of FERS was compared with conventional cuvette measurements with identical experimental parameters (cuvette volume 200 μL).

The Raman spectra of the solutions contained a background signal contributed by the solvent. In order to achieve reproducibility for precise quantification, the measured

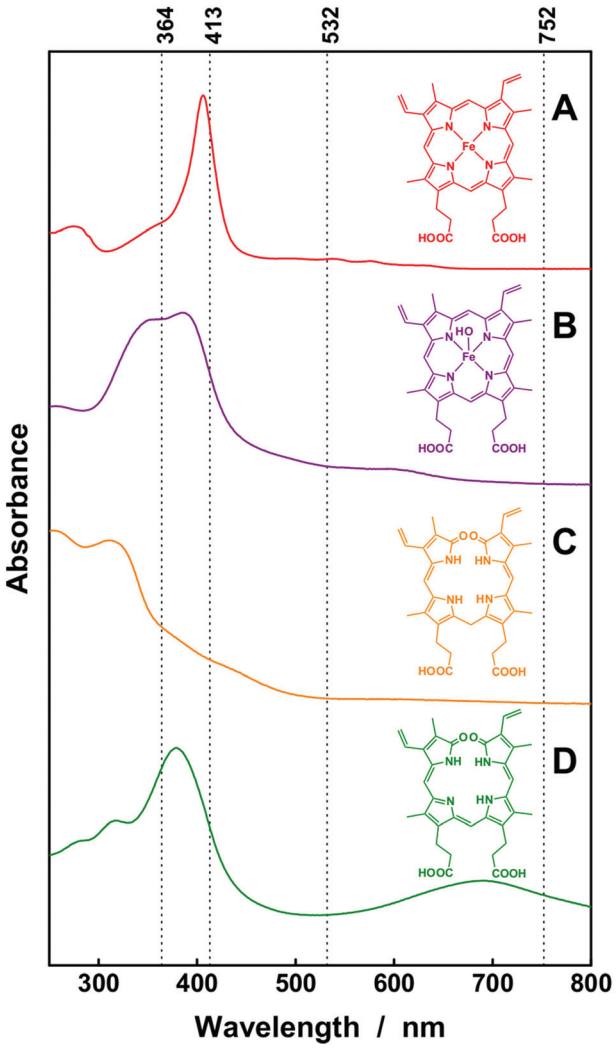

Fig. 2 Schematic chemical structures and absorption spectra in aqueous solution of the heme chromophores: chemical structures of hemoglobin (A), hematin (B), bilirubin (C) and biliverdin (D), respectively. The simplified heme structure represents the chromophoric unit of hemoglobin. The applied laser excitation wavelengths $\lambda_{exc.}$ = 364 nm, $\lambda_{exc.}$ = 413 nm, $\lambda_{exc.}$ = 532 nm, and $\lambda_{exc.}$ = 752 nm are depicted as vertical dashed lines. These selected excitation wavelengths can be carefully tuned into the electronic absorption bands of the individual chromophores and strong resonance Raman enhancements can be achieved for the vibrational modes that are coupled to these electronic transitions.

Raman spectra were normalized to the Raman band of the solvent water at 1645 cm^{-1} and/or the band of the phosphate buffer at approximately 990 cm^{-1}. As the analyte concentrations were extremely low, the quantity of the solvent could be considered as constant in all solutions. Thus, the Raman peak of water and/or the signal of the buffer was utilized as an internal standard[27,28] to cancel out all random factors (fluctuations in laser intensity and optical coupling, *etc.*) and to improve the quantitative detection ability. The signal-to-noise ratio (SNR) was calculated from the height of the Lorenzian fit of the target peaks and the root-mean-square (RMS) values of

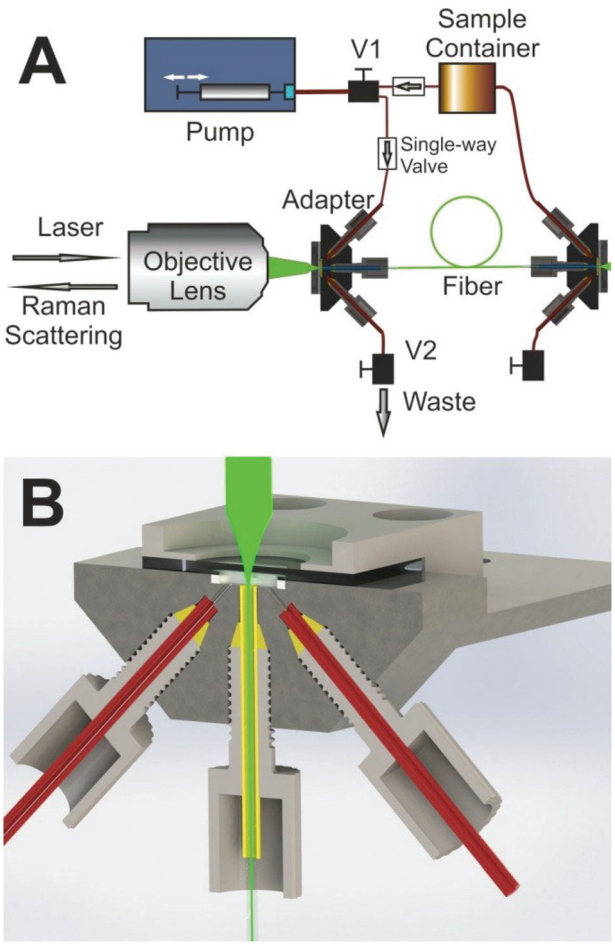

Fig. 3 A: Scheme of the fiber enhanced Raman spectroscopic (FERS) setup, consisting of laser, objective lens, fiber with adapter assembly, pump, and spectrometer. B: Detail of the fiber adapter assembly. The laser light is coupled through an optical window into the fiber hollow core and the analyte solution is pumped through the hollow core by side connectors.

the baseline. The lowest detectable concentrations were derived when the SNR was equal to three.

Estimating the potential of FERS for ultrasensitive analysis

The attenuation that is introduced by the samples and the fiber were thoroughly discussed.[27] The back scattered Raman intensity in an absorbing liquid core fiber can be expressed as following:

$$I_R(\tilde{\upsilon}, c) = A' \cdot I_0 \cdot \sigma(\tilde{\upsilon}) \cdot e^{-((\varepsilon_l + \varepsilon_r) \cdot c \cdot L_d)} \cdot \frac{1 - e^{-(\mu_{sl} + \mu_{sr} + (\varepsilon_l + \varepsilon_r) \cdot c) \cdot L_p}}{\mu_{sl} + \mu_{sr} + (\varepsilon_l + \varepsilon_r) \cdot c} \cdot c \quad (1)$$

In this equation, A' represents the efficiency of the instrument, I_0 the laser intensity, $\sigma(\tilde{\upsilon})$ the Raman scattering cross section, c the analyte concentration, $\mu_{sl}(\lambda)$ and $\mu_{sr}(\lambda)$ the effective scattering loss coefficients that account for waveguide imperfections at the laser and the Raman wavelengths, while $\varepsilon_l(\lambda)$ and $\varepsilon_r(\lambda)$ account for the analyte extinction coefficients at the wavelengths of the laser and the Raman scattered radiation.[27]

Eqn (1) can be simplified to a function (2) of concentration with the parameters A, B, C and the constants L_d and L_p.[27]

$x = c$; $y = I_R(\tilde{\upsilon},x)$; $A = A' \cdot I_0 \cdot \sigma(\tilde{\upsilon})$; $B = \varepsilon_l + \varepsilon_r$; $C = \mu_{sl} + \mu_{sr}$; $L_d = 1$ mm; $L_p = 400$ mm.

$$y = A \cdot e^{-(B \cdot x \cdot L_d)} \cdot \frac{1 - e^{-(C + Bx) \cdot L_p}}{C + Bx} \cdot x \quad (2)$$

Eqn (2) was applied for non-linear fitting of the experimentally derived data.

Vibrational assignment of Raman marker bands with help of density functional theory calculation

In order to give an assignment and interpretation of the Raman marker bands that were utilized for the detection of bilirubin and biliverdin, a thorough calculation of the molecular structures, vibrational modes, and Raman activities was performed with help of density functional theory calculations with Gaussian 09.[29] Hybrid exchange correlation functionals were applied with Becke's three-parameter exchange functional[30] (B3) as slightly modified by Stephens *et al.*[31] coupled with the correlation part of the functional from Lee, Yang, and Parr (B3LYP)[32] and Dunnings triple (cc-pVTZ) correlation consistent basis sets[33] of contracted Gaussian functions with polarized and diffuse functions.[34] The solvent water was simulated with the polarizable continuum model (PCM). The comparison of the calculated Raman spectra with the FT-Raman spectra of bilirubin and biliverdin is shown in the ESI (Fig. S1†).

Results and discussion

Raman spectroscopy is a chemically selective, non-invasive technique[35] that has evolved as an extremely powerful analytical tool for studying the structural properties of biomolecules[36] and their interaction with pharmaceuticals.[37] Because of the weak inelastic Raman scattering, various elaborated enhancement techniques have been developed, such as resonance Raman spectroscopy (RRS) and fiber enhanced Raman spectroscopy (FERS). In order to study these enhancements thoroughly, several laser excitation wavelengths have been chosen. The wavelengths λ = 413 nm and λ = 364 nm match the strong Soret band[38] of hematin and the electronic absorption bands of biliverdin and bilirubin, respectively (Fig. 2). Therefore, a strong signal enhancement of vibrational modes that are coupled to these electronic transitions is expected in resonance Raman spectroscopy.[3a] By exciting and collecting the Raman signals of the analytes within the hollow cores of elaborated optical fibers, a strong signal enhancement can be achieved.[39]

Fiber enhanced Raman spectroscopy of hematin, hemoglobin, and whole erythrocytes

First, the ability of fiber enhanced resonance Raman spectroscopy as an analytical tool for the highly sensitive quantification of heme was studied thoroughly. The laser excitation wavelength λ = 532 nm (Fig. 2) was applied for analyzing the

enhancement provided by the fiber guiding. The strong peak of hematin in the Raman spectrum at 1626 cm^{-1}, which is assigned to the vibrational mode ν_{10},[3a,d] was detected with identical laser power and spectrometer setting in a series of concentration in conventional cuvette measurements and in fiber enhanced Raman sensing. The intensities of this Raman peak were analyzed for quantification of the limit-of-detection (LOD, 3× noise std.) of hematin as 36 μM and 3.6 μM, for conventional and fiber measurement respectively (Table 1). In order to exploit an additional resonance Raman enhancement, the excitation wavelength λ = 413 nm was applied, which matches the strong electronic absorption of hematin (Fig. 2B). The molecular vibration at 1373 cm^{-1}, which is assigned to the totally symmetric mode ν_4,[3a,d,e] was strongly enhanced with this wavelength. Thus a significantly improved LOD of only 0.1 μM was achieved with fiber enhanced resonance Raman spectroscopy and only 0.9 pmol sample was needed (Table 1). The spectra of hematin showed an excellent linearity between the Raman signal intensity and the analyte concentration, thus providing a reproducible quantification method. With help of this calibration, one can now measure the Raman signal of an unknown sample and quantify the actual hematin concentration.

In the next step, a more complex structure, hemoglobin was analyzed. Conventional and enhanced Raman spectra of hemoglobin were recorded respectively. The Raman band at 1373 cm^{-1} of hemoglobin, which was assigned to mode ν_4 of the heme group,[36e] was significantly enhanced in the fiber enhanced resonance Raman spectra. This Raman peak is also a very interesting marker band for monitoring the hemoglobin oxidation state,[36e,40] which provides additional information about the oxygenation of the monitored blood, and supports a differential diagnosis. The spectroscopic analysis shows that the LODs of heme were improved from 10.7 μM for conventional measurements with λ = 532 nm excitation down to 0.25 μM in fiber enhanced resonance Raman sensing. An excellent linearity was achieved for reliable quantification of hemoglobin (Fig. 4A). Fiber enhanced Raman sensing provided a higher sensitivity, which is seen in the steeper slope of the linear fits (Fig. 4A and B compared to Fig. 4C and D). Thus, FERS is capable of measuring very low hematin and hemoglobin concentrations that are not detectable anymore with conventional Raman measurements.

In order to prove the potential of FERS for investigating complex biological samples, also whole, intact erythrocytes were analyzed. Photodegradation of the red blood cells was very well avoided due to continuous analyte flow and the short time in the laser focus. Raman spectra of intact, oxygenated erythrocytes were nicely recorded with FERS (Fig. 5). In the resonance Raman spectra of the erythrocytes with λ = 413 nm excitation (Fig. 5A), the strongest Raman peak at 1376 cm^{-1} corresponds to the vibrational mode ν_4. This vibrational mode was not as strong in the Raman spectra excited with λ = 532 nm (Fig. 5B), in very good agreement to the pure hemoglobin spectra. Thus, fiber enhanced resonance Raman spectroscopy showed promising compatibility with delicate biological cells, such as intact oxygenated erythrocytes and has great potential for medical diagnosis of red blood cell related diseases, for example different types of anemia and hemolytic disorders.

Quantification and monitoring of the degradation products biliverdin and bilirubin and demonstration of the potential of FERS as diagnostic tool

The heme prostetic groups of hemoglobin in the erythrocytes are enzymatically degraded into biliverdin which is further reduced to bilirubin. These two molecules are found as the major metabolites of the porphyrine ring. As bilirubin is a quite reactive molecule, it is normally detoxified by glucuronidisation in the liver and then eliminated *via* bile. Still, in many diseases an elevated serum level of unconjugated bilirubin and/or biliverdin can be observed.[6,11–13,14b,41]

The bile pigments, biliverdin and bilirubin, cause extremely strong fluorescence signals with most excitation wavelengths in the ultraviolet and visible range and therefore Raman sensing was very challenging (data not shown). A thorough examination elucidated that the fluorescence signal was not obvious with excitation wavelength λ = 364 nm. Strong resonance enhancements can be achieved with this wavelength for bilirubin (Fig. 2C) and biliverdin (Fig. 2D) and the Raman bands around at 1615 cm^{-1} can be exploited as marker peaks for ultrasensitive analysis of biliverdin and bilirubin, respectively. The Raman spectra were strongly enhanced by applying FERS (Fig. 6A and B) and LODs of 0.13 μM and 0.5 μM were achieved for biliverdin and for bilirubin, respectively (Table 1). A good linearity between the Raman signal intensity and the

Table 1 Comparison of the improvement in the quantification of hematin, hemoglobin, biliverdin, and bilirubin in the cases of conventional (Conv.) and fiber enhanced Raman spectroscopy (FERS). The intensities of the chosen laser wavelengths were different ($I_{\lambda=413\ nm}$ = 7 mW, $I_{\lambda=532\ nm}$ = 10 mW, and $I_{\lambda=364\ nm}$ = 3.5 mW) and all values were scaled to 7 mW ($I_{\lambda=413\ nm}$) for better comparison. The amount of substance for each method was derived from the limit-of-detection (LOD) and the required sample volume

	Hematin				Hemoglobin				Biliverdin		Bilirubin	
$\lambda_{exc.}$	413 nm		532 nm		413 nm		532 nm		364 nm		364 nm	
Method	Conv.	FERS	Conv.	FERS	Conv.	FERS	Conv.	FERS	Conv.	FERS	Conv.	FERS
LOD (μM)	1	0.1	35.71	3.57	2.50	0.25	10.71	1.43	1.25	0.13	12.50	0.50
Amount (pmol)	200	0.9	7142	32.13	500	2.25	2142	12.87	250	1.17	2500	4.5

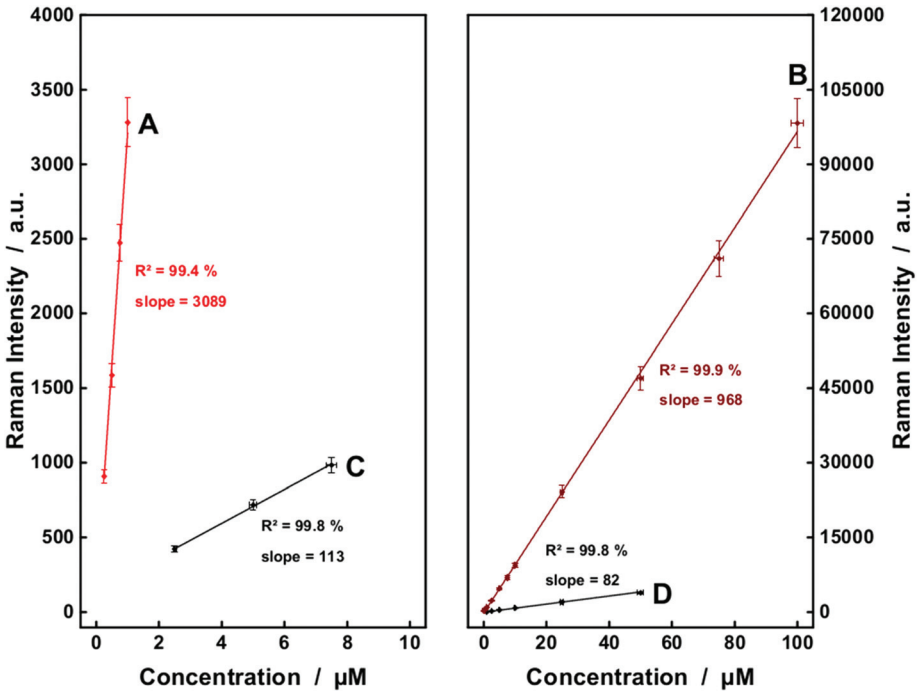

Fig. 4 Comparison of fiber enhanced Raman spectra of hemoglobin (A) and hematin (B) with conventional Raman detection of hemoglobin (C) and hematin (D) in aqueous solutions with $\lambda_{exc.}$ = 413 nm. The Raman intensities with $\lambda_{exc.}$ = 413 nm were defined by the peak heights of the Raman bands at 1373 cm^{-1} for both hematin and hemoglobin. For measurements with $\lambda_{exc.}$ = 532 nm (not shown), the Raman bands at 1626 cm^{-1} and 1638 cm^{-1} were chosen for hematin and hemoglobin, respectively.

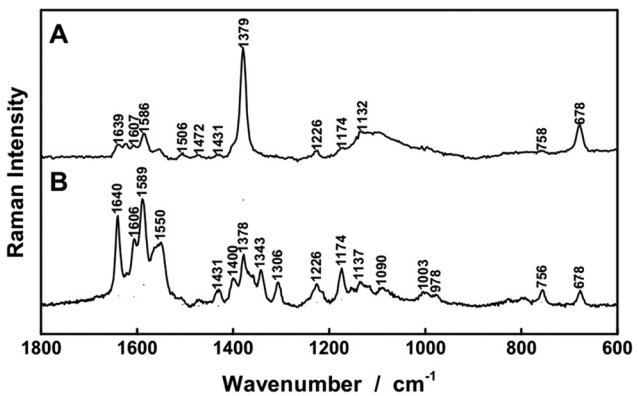

Fig. 5 Fiber enhanced Raman spectra of whole erythrocytes. Intact red blood cells (1 : 199 diluted in 1× PBS) were gently guided through the hollow core fiber and Raman spectra were taken with $\lambda_{exc.}$ = 413 nm (A) and $\lambda_{exc.}$ = 532 nm (B).

concentration was obtained, proving the potential of FERS as an analytical tool for the diagnosis of different types of diseases manifested in jaundice.[6,12] Especially the rare, not yet well understood diseases manifested in hyperbiliverdinemia[12,13,14b] need a novel tool for simultaneous sensing of very low amounts biliverdin, reported as 0.9–6.5 µM (ref. 13) and in the range from 1–10% of the total bilirubin value.[14b]

Thus, first a two component solution, consisting of 1 µM biliverdin and 50 µM bilirubin was analyzed in order to simulate typical concentrations of patients presenting hyperbilirubinemia.[13] The Raman spectra of biliverdin and bilirubin share most of the strong peaks with excitation λ = 364 nm due to the similarity in their molecular structure (Fig. 2C and D). However, some Raman bands in the wavenumber range between 1220 cm^{-1} and 1300 cm^{-1} are different and can be decomposed (Fig. 6E–G). Bilirubin contains a peak in the Raman spectrum at 1272 cm^{-1}, which is assigned to a combination of CC-stretching vibration in one pyrrole unit as well as CH-, CH_3-, and OH-wagging and scissoring vibrations (Fig. 7A). The Raman band of biliverdin at 1282 cm^{-1} can be assigned to a combined vibration which is distributed across the whole molecule and consists of strong CC- and CN-stretching vibrations in several pyrrole units as well as CH-, CH_2-, and OH-wagging and scissoring vibrations (Fig. 7B). The height of the peak at 1272 cm^{-1} in the pure Raman spectrum of a 100 µM solution of bilirubin (Fig. 6E) was quantified to 2423 counts (arbitrary units) and the height of the peak at 1282 cm^{-1} in the pure Raman spectrum of a 1 µM solution of biliverdin (Fig. 6F) was quantified to 1177 counts (arbitrary units). By deconvolution of the Raman spectrum of the two component solution (1 µM biliverdin and 50 µM bilirubin, Fig. 6G), the peak heights of the 1272 cm^{-1} and 1282 cm^{-1} bands were quantified to 1367 ± 198 and 1126 ± 212 counts (arbitrary units), respectively. Therefore, the measured concentrations were 0.9(6) ± 0.2 µM for biliverdin and 56 ± 8 µM for bilirubin. These results nicely demonstrate that FERS can be applied in the analysis of hyperbilirubinemia to quantify con-

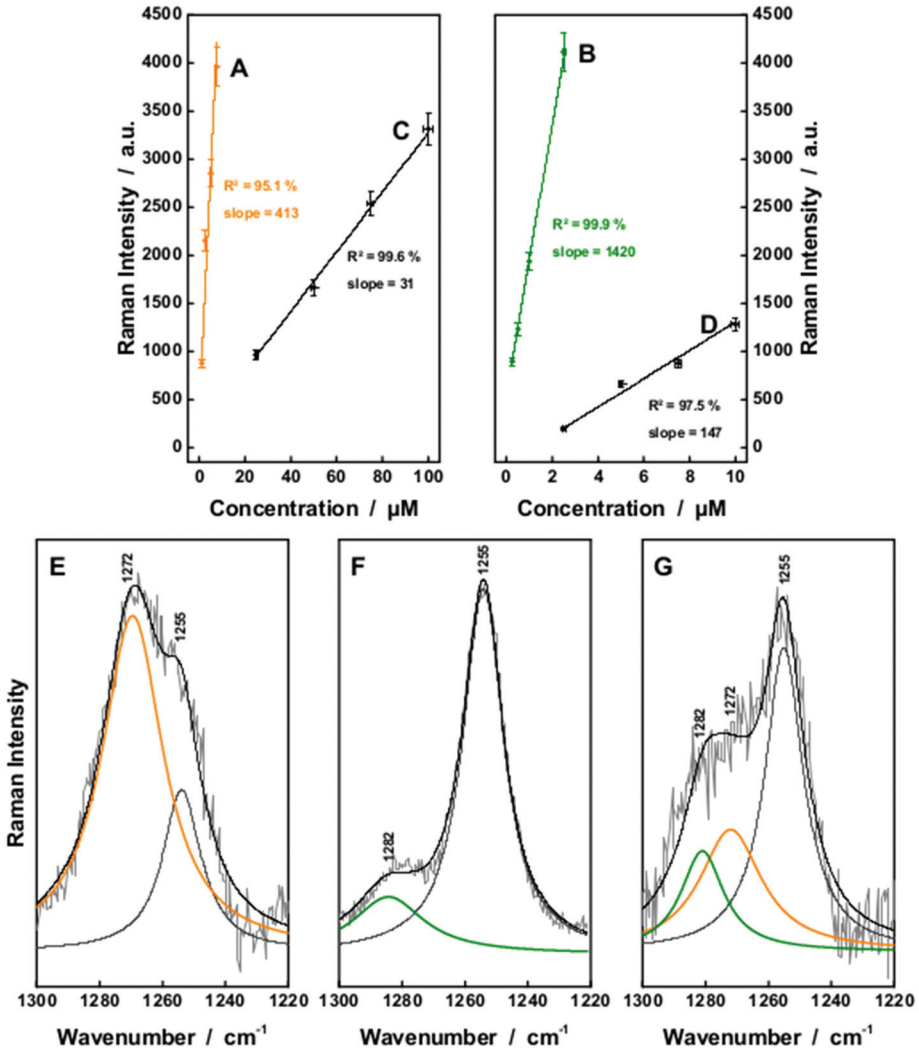

Fig. 6 The fiber enhanced and conventional Raman detection of aqueous solutions of bilirubin (A and C) as well as biliverdin (B and D) was compared with $\lambda_{exc.}$ = 364 nm. A lower limit of detection was achieved by FERS. The resonance Raman spectra of the chemically similar chromophores can be distinguished within the wavenumber range between 1220 and 1300 cm^{-1} as shown in comparison of the Raman spectra of bilirubin (E), biliverdin (F) and a mixture of 1 µM biliverdin and 50 µM bilirubin (G). Both chromophores can be quantified simultaneously in a mixture of both substances. The whole Raman spectra are given in the ESI (Fig. S2†).

centrations of biliverdin at 1 µM alongside concentrations of bilirubin at 50 µM.

For higher biliverdin concentrations of patients presenting hyperbiliverdinemia,[13] also non-resonant FERS at $\lambda_{exc.}$ = 752 nm (Fig. 2) can be applied in order to analyze a two component solution which contains 25 µM bilirubin and 75 µM biliverdin, as present in the case of green jaundice.[13] The individual solutions of 25 µM bilirubin (Fig. 8A) and 75 µM biliverdin (Fig. 8B) were thoroughly analyzed and the Raman peaks at 1253 cm^{-1} (bilirubin) and 1243 cm^{-1} (biliverdin) were identified as suitable marker bands, in order to distinguish both bile pigments. The molecular vibration of bilirubin at 1253 cm^{-1} is assigned to CH-, NH-, and OH-bending vibrations (Fig. 7C). The Raman band of biliverdin at 1243 cm^{-1} consists of CH, NH, and OH-bending vibrations (Fig. 7D). By deconvolution of the Raman spectrum of the two component mixture (Fig. 8C), the peak heights of the 1253 cm^{-1} and 1243 cm^{-1} bands in the spectrum of the mixture were quantified to 2516 ± 94 and 26 135 ± 863 counts (arbitrary units), respectively. Thus the concentrations were calculated to be 24.1 ± 1.8 µM for bilirubin and 77.2 ± 5.0 µM for biliverdin in very good agreement to the theoretical values. Hence, FERS is also a powerful technique for the analysis of the concentrations of bile pigments which appear in case of hyperbiliverdinemia.[13]

Potential of FERS for ultrasensitive analysis of heme and bile pigments

Finally, the potential of FERS was estimated considering further improvements for ultrasensitive analysis of heme and the bile pigments. The original height of the hematin peak at 1373 cm^{-1} was analyzed alongside the non-linear fitting based

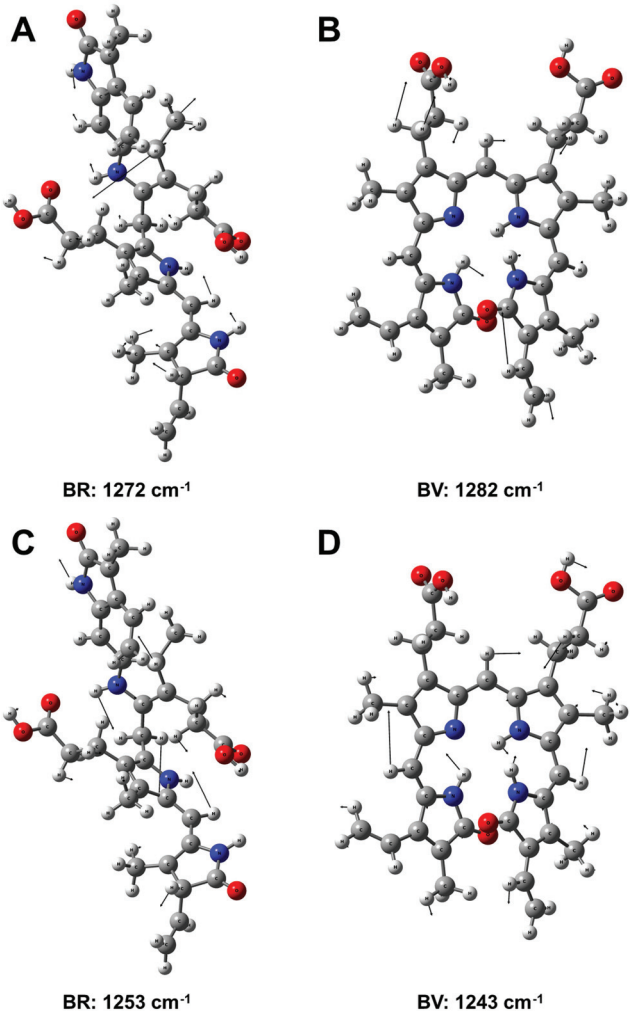

Fig. 7 Assignment of the vibrational modes of bilirubin (BR) and biliverdin (BV) that were used as Raman marker bands for sensing these molecules (see Fig. 6 and 8). The atomic displacements of the associated vibrational modes are A: BR at 1272 cm^{-1}, B: BV at 1282 cm^{-1}, C: BR at 1253 cm^{-1} and D: BV at 1243 cm^{-1}. The Raman bands originate from combined stretching and bending modes across the molecules.

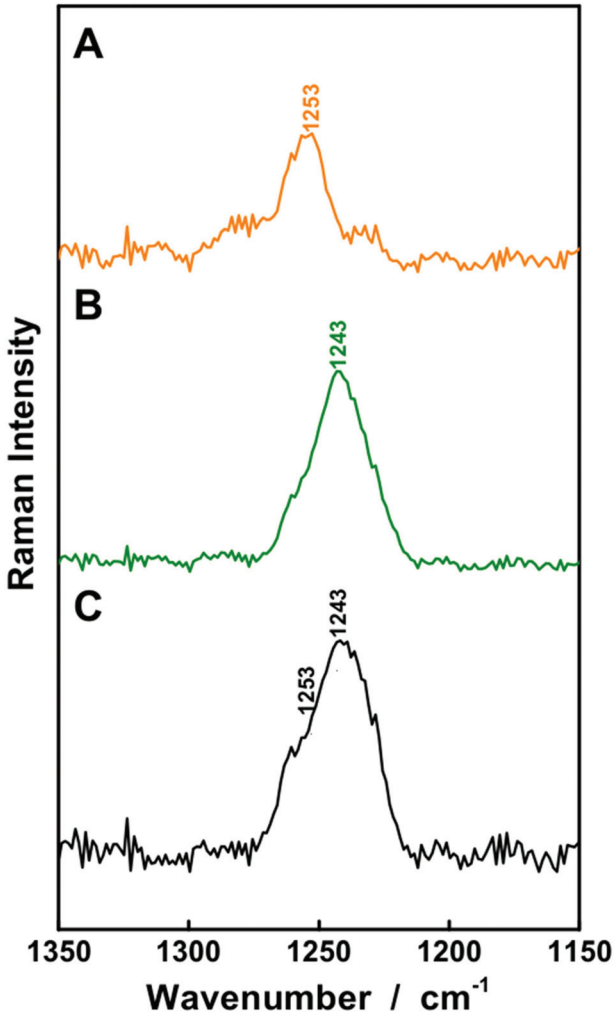

Fig. 8 Raman spectra of a 25 μM aqueous solution of pure bilirubin (A), a 75 μM aqueous solution of pure biliverdin (B), and a mixture of 25 μM bilirubin and 75 μM biliverdin (C) with $\lambda_{exc.}$ = 752 nm. The Raman bands at 1243 cm^{-1} and at 1253 cm^{-1} were utilized for the calculation of the concentrations of biliverdin and bilirubin in the mixture. The experimentally derived concentrations were 24.1 μM bilirubin (4% error) and 77.2 μM biliverdin (3% error), respectively.

on eqn (2). The peak intensities fit very well to the theoretical prediction (A = 27.6 ± 7.36 arb. unit; B = 0.00416 ± 0.00062 μM^{-1} mm^{-1}; C = 0.115 ± 0.046 mm^{-1}). The extinction coefficient of the liquid sample, which was derived as parameter B in the fitting function, is also very close to that adapted from absorption spectrum:

$$B_{\text{measured}} = \varepsilon_{\text{excitation}} + \varepsilon_{\text{Raman peak}} = 0.00413\ \mu M^{-1}\ mm^{-1}.$$

The original peak height of bilirubin had the same trend. The non-linear fitting based on eqn (2) derived the values A = 25.0 ± 0.4 arb. unit; B = 0.00325 ± 0.00067 μM^{-1} mm^{-1}; C = 0.0914 ± 0.0057 mm^{-1}. The parameter B adapted from the absorption spectrum of bilirubin solution (B_{measured} = 0.00350 μM^{-1} mm^{-1}) was in very good agreement to the calculated value.

The function of the Raman intensity $I_R(\tilde{\nu},c)$ is defined by five factors:[27] A, B, C, L_d, and L_p. Factor A expresses the intensity of the excitation laser and the overall performance of the optical coupling and sensing. Factor B is defined by the optical property of the sample and becomes larger when stronger absorbing samples are utilized. Parameter C is depending on the wave-guiding quality of the fiber. In case of ultra-low-concentration sensing, the value of x is extremely small and the influence of parameters B and L_d is minimized as they appear together with the analyte concentration. Thus, in further work it will be worth to develop fiber systems with better parameter C and larger L_p, or in other words, liquid-core fibers with superior guiding property and sufficient length.

Based on eqn (2), with improved parameters A = 20 000 arb. unit, B = 0.00416 μM^{-1} mm^{-1}, C = 0.0005 mm^{-1},

L_p = 4000 mm, L_d = 1 mm, one can predict an improved LOD of hematin of 1.3 pM. The accordingly predicted LODs of bilirubin and biliverdin are 66 pM and 1.6 pM, respectively.

Hence, FERS is a promising technique for rapid monitoring of slight variations of the bilirubin level at extremely low sample demand, which would be of utmost importance for an early diagnosis of mild hyperbilirubinemia in neonates[7–11] and the Gilbert[5c] and Crigler–Najjar syndrome[5d] as well as in cancer research[16a,20] and to elucidate the role of the bile pigments in brain-processes.[1]

Conclusion

This work explores the analytical potential of fiber enhanced resonance Raman spectroscopy (FERS) for ultrasensitive analysis of biologically important heme chromophores and for future applications in the diagnosis and monitoring of hyperbilirubinemia and hyperbiliverdinemia related diseases by the analysis of minimal amounts of bile pigments.

Hematin and hemoglobin were traced down to concentrations of 0.1 μM and 0.25 μM at very low sample demands of 0.9 pmol and 2.25 pmol, respectively. The FERS setup provided an excellent linearity between signal intensity and heme concentration and allowed for robust quantification of hematin and hemoglobin concentrations that were not detectable anymore with conventional Raman measurements. An improved limit of detection of only 1.3 pM hematin could be achieved based on modelling the setup performance with improved optical fibers. In order to demonstrate the abilities of the FERS technique for measuring whole cells, also intact, oxygenated erythrocytes were successfully analyzed in the hollow core optical fibers, demonstrating the great potential for medical diagnosis of red blood cell related diseases, for example different types of anemia and hemolytic disorders.

Considering the small sample volume demand of only few microliters, FERS would perfectly suit the requirements on a minimal invasive procedure for bilirubin concentration level monitoring in neonatal jaundice[11] by using capillary blood samples and for an early diagnosis of the Gilbert[5c] and Crigler–Najjar[5d] syndrome. The bile pigments biliverdin and bilirubin were quantified down to LODs of 0.13 μM and 0.5 μM, with proposed improvements down to 1.6 pM and 66 pM. This precise detection of minor elevations of the biliverdin and bilirubin levels in the micro-molar concentration range, can also open up a new prospective for further research regarding cancer and oxidative stress. Recently, efforts have been made for understanding the relationship between heme oxygenase-1 (the enzyme that converts heme to biliverdin) and the brain function.[1] With the discussed prospects for a detection of pico-molar concentration changes, a new analytical method would be available for a better understanding of the role of the bile pigments (especially biliverdin) in processes in the brain.[1]

In order to demonstrate the potential of FERS as a diagnostic tool, clinical relevant bilirubin and biliverdin concentrations were thoroughly quantified for the case of hyperbilirubinemia due to malignancy, infectious hepatitis, cirrhosis or stenosis of the common bile duct (1 μM biliverdin together with 50 μM bilirubin)[13,14b] and for hyperbiliverdinemia (75 μM biliverdin and 25 μM bilirubin).[13] Hence, FERS is a new method being capable to promote a better diagnosis.

In summary, FERS is a chemical selective, ultrasensitive technique, with extremely low sample demand and has remarkable potential for a wide range of life-science applications. The analytical benchmark experiments in this contribution provide the foundation for future clinical studies.

Acknowledgements

Funding from the federal state of Thuringia and European Union (EFRE) is highly acknowledged (2015 FE 9012 and 2015-0021). Computations at the computing centre of University Leipzig are highly acknowledged. T. F. is grateful for support from the "Studienstiftung des deutschen Volkes". M. W. P. was supported by a grant from the German Ministry of Education and Research (01KI1501).

Notes and references

1 L. Zhang, *Heme Biology: The Secret Life of Heme in Regulating Diverse Biological Processes*, World Scientific Publishing Company, 2011.

2 M. F. Perutz, M. G. Rossmann, A. F. Cullis, H. Muirhead, G. Will and A. C. T. North, Structure of Haemoglobin: A Three-Dimensional Fourier Synthesis at 5.5-[angst]. Resolution, Obtained by X-Ray Analysis, *Nature*, 1960, **185**(4711), 416–422.

3 (*a*) B. R. Wood, S. J. Langford, B. M. Cooke, J. Lim, F. K. Glenister, M. Duriska, J. K. Unthank and D. McNaughton, Resonance Raman spectroscopy reveals new insight into the electronic structure of beta-hematin and malaria pigment, *J. Am. Chem. Soc.*, 2004, **126**(30), 9233–9239; (*b*) T. Frosch, B. Küstner, S. Schlücker, A. Szeghalmi, M. Schmitt, W. Kiefer and J. Popp, In vitro polarization-resolved resonance Raman studies of the interaction of hematin with the antimalarial drug chloroquine, *J. Raman Spectrosc.*, 2004, **35**(10), 819–821; (*c*) T. Frosch, S. Koncarevic, K. Becker and J. Popp, Morphology-sensitive Raman modes of the malaria pigment hemozoin, *Analyst*, 2009, **134**(6), 1126–1132; (*d*) T. Frosch, S. Koncarevic, L. Zedler, M. Schmitt, K. Schenzel, K. Becker and J. Popp, In Situ Localization and Structural Analysis of the Malaria Pigment Hemozoin, *J. Phys. Chem. B*, 2007, **111**(37), 11047–11056; (*e*) S. Cînta-Pînzaru, N. Peica, B. Küstner, S. Schlücker, M. Schmitt, T. Frosch, J. H. Faber, G. Bringmann and J. Popp, FT-Raman and NIR-SERS characterization of the antimalarial drugs chloroquine and mefloquine and their interaction with hematin, *J. Raman Spectrosc.*, 2006, **37**(1–3), 326–334; (*f*) M. Brückner,

K. Becker, J. Popp and T. Frosch, Fiber array based hyperspectral Raman imaging for chemical selective analysis of malaria-infected red blood cells, *Anal. Chim. Acta*, 2015, **894**, 76–84.

4 G. Kikuchi, T. Yoshida and M. Noguchi, Heme oxygenase and heme degradation, *Biochem. Biophys. Res. Commun.*, 2005, **338**(1), 558–567.

5 (*a*) R. H. Tukey and C. P. Strassburg, Human UDP-glucuronosyltransferases: metabolism, expression, and disease, *Annu. Rev. Pharmacol. Toxicol.*, 2000, **40**(1), 581–616; (*b*) A. W. Wolkoff, in *Inheritable disorders manifested by conjugated hyperbilirubinemia*, Seminars in Liver Disease, © 1983 by Thieme Medical Publishers, Inc., 2008, pp. 65–72; (*c*) P. J. Bosma, J. R. Chowdhury, C. Bakker, S. Gantla, A. de Boer, B. A. Oostra, D. Lindhout, G. N. Tytgat, P. L. Jansen and R. P. O. Elferink, The genetic basis of the reduced expression of bilirubin UDP-glucuronosyltransferase 1 in Gilbert's syndrome, *N. Engl. J. Med.*, 1995, **333**(18), 1171–1175; (*d*) I. J. Fox, J. R. Chowdhury, S. S. Kaufman, T. C. Goertzen, N. R. Chowdhury, P. I. Warkentin, K. Dorko, B. V. Sauter and S. C. Strom, Treatment of the Crigler–Najjar Syndrome Type I with Hepatocyte Transplantation, *N. Engl. J. Med.*, 1998, **338**(20), 1422–1427.

6 D. D. Houlihan, M. J. Armstrong and P. N. Newsome, Investigation of jaundice, *Medicine*, 2011, **39**(9), 518–522.

7 S. W. Ryter, Bile pigments in pulmonary and vascular disease, *Front. Pharmacol.*, 2012, **3**, 39.

8 L. Vitek and J. D. Ostrow, Bilirubin chemistry and metabolism; harmful and protective aspects, *Curr. Pharm. Des.*, 2009, **15**(25), 2869–2883.

9 M. Kaplan and C. Hammerman, Understanding severe hyperbilirubinemia and preventing kernicterus: adjuncts in the interpretation of neonatal serum bilirubin, *Clin. Chim. Acta*, 2005, **356**(1), 9–21.

10 D. Zakim, T. D. Boyer, M. P. Manns and A. J. Sanyal, *Zakim and Boyer's Hepatology*, Elsevier Health Sciences, 2011, 1096–1097.

11 J. M. Kirk, Neonatal jaundice: a critical review of the role and practice of bilirubin analysis, *Ann. Clin. Biochem.*, 2008, **45**(5), 452–462.

12 E. A. Larson, G. T. Evans and C. J. Watson, A study of the serum biliverdin concentration in various types of jaundice, *J. Lab. Clin. Med.*, 1947, **32**(5), 481.

13 M. Gåfvels, P. Holmström, A. Somell, F. Sjövall, J. O. Svensson, L. Ståhle, U. Broomé and P. Stål, A novel mutation in the biliverdin reductase-A gene combined with liver cirrhosis results in hyperbiliverdinaemia (green jaundice), *Liver Int.*, 2009, **29**(7), 1116–1124.

14 (*a*) S. M. Purcell, F. H. Wians Jr., N. B. Ackerman Jr. and B. M. Davis, Hyperbiliverdinemia in the bronze baby syndrome, *J. Am. Acad. Dermatol.*, 1987, **16**(1), 172–177; (*b*) A. J. Greenberg, I. Bossenmaier and S. Schwartz, Green jaundice, *Am. J. Dig. Dis.*, 1971, **16**(10), 873–880; (*c*) J. Prichard, Biliverdin appearing in a case of malnutrition, *Br. J. Clin. Pract.*, 1972, **26**(10), 481.

15 (*a*) L. J. Horsfall, G. Rait, K. Walters, D. M. Swallow, S. P. Pereira, I. Nazareth and I. Petersen, Serum bilirubin and risk of respiratory disease and death, *JAMA, J. Am. Med. Assoc.*, 2011, **305**(7), 691–697; (*b*) E. H. Temme, J. Zhang, E. G. Schouten and H. Kesteloot, Serum bilirubin and 10-year mortality risk in a Belgian population, *Cancer Causes Control*, 2001, **12**(10), 887–894.

16 (*a*) A. C. Bulmer, K. Ried, J. T. Blanchfield and K.-H. Wagner, The anti-mutagenic properties of bile pigments, *Mutat. Res., Rev. Mutat. Res.*, 2008, **658**(1), 28–41; (*b*) Y. Katoh, N. Nemoto, M. Tanaka and S. Takayama, Inhibition of benzo [*a*] pyrene-induced mutagenesis in Chinese hamster V79 cells by hemin and related compounds, *Mutat. Res. Lett.*, 1983, **121**(2), 153–157.

17 F. McPhee, P. Caldera, G. Bemis, A. McDonagh, I. Kuntz and C. Craik, Bile pigments as HIV-1 protease inhibitors and their effects on HIV-1 viral maturation and infectivity in vitro, *Biochem. J.*, 1996, **320**, 681–686.

18 P. Rao, R. Suzuki, S. Mizobuchi, T. Yamaguchi and S. Sasaguri, Bilirubin exhibits a novel anti-cancer effect on human adenocarcinoma, *Biochem. Biophys. Res. Commun.*, 2006, **342**(4), 1279–1283.

19 P. Keshavan, S. J. Schwemberger, D. L. Smith, G. F. Babcock and S. D. Zucker, Unconjugated bilirubin induces apoptosis in colon cancer cells by triggering mitochondrial depolarization, *Int. J. Cancer*, 2004, **112**(3), 433–445.

20 Y. Katoh, N. Nemoto, M. Tanaka and S. Takayama, Inhibition of Benzo[a]Pyrene-Induced Mutagenesis in Chinese-Hamster V79-Cells by Hemin and Related-Compounds, *Mutat. Res.*, 1983, **121**(2), 153–157.

21 M. Prezelj, Enzymic determination of total bilirubin in serum with the BA-1000, *Clin. Chem.*, 1988, **34**(1), 176–177.

22 B. T. Doumas, B. W. Perry, E. A. Sasse and J. V. Straumfjord, Standardization in bilirubin assays: evaluation of selected methods and stability of bilirubin solutions, *Clin. Chem.*, 1973, **19**(9), 984–993.

23 (*a*) X. Li and Z. Rosenzweig, A fiber optic sensor for rapid analysis of bilirubin in serum, *Anal. Chim. Acta*, 1997, **353**(2), 263–273; (*b*) C. Lu, J.-M. Lin and C. W. Huie, Determination of total bilirubin in human serum by chemiluminescence from the reaction of bilirubin and peroxynitrite, *Talanta*, 2004, **63**(2), 333–337.

24 (*a*) C.-Y. Huang, M.-J. Syu, Y.-S. Chang, C.-H. Chang, T.-C. Chou and B.-D. Liu, A portable potentiostat for the bilirubin-specific sensor prepared from molecular imprinting, *Biosens. Bioelectron.*, 2007, **22**(8), 1694–1699; (*b*) M. A. Rahman, K.-S. Lee, D.-S. Park, M.-S. Won and Y.-B. Shim, An amperometric bilirubin biosensor based on a conductive poly-terthiophene–Mn (II) complex, *Biosens. Bioelectron.*, 2008, **23**(6), 857–864.

25 (*a*) J. J. Lauff, M. E. Kasper and R. T. Ambrose, Separation of bilirubin species in serum and bile by high-performance reversed-phase liquid chromatography, *J. Chromatogr. B: Biomed. Sci. Appl.*, 1981, **226**(2), 391–402; (*b*) J. J. Lauff, M. E. Kasper, T. W. Wu and R. T. Ambrose, Isolation and

preliminary characterization of a fraction of bilirubin in serum that is firmly bound to protein, *Clin. Chem.*, 1982, **28**(4), 629–637.

26 (*a*) B. J. Marquardt, P. G. Vahey, R. E. Synovec and L. W. Burgess, A Raman waveguide detector for liquid chromatography, *Anal. Chem.*, 1999, **71**(21), 4808–4814; (*b*) M. J. Pelletier and R. Altkorn, Raman sensitivity enhancement for aqueous protein samples using a liquid-core optical-fiber cell, *Anal. Chem.*, 2001, **73**(6), 1393–1397; (*c*) R. Altkorn, I. Koev and M. J. Pelletier, Raman Performance Characteristics of Teflon®-AF 2400 Liquid-Core Optical-Fiber Sample Cells, *Appl. Spectrosc.*, 1999, **53**(10), 1169–1176; (*d*) R. Altkorn, M. D. Malinsky, R. P. Van Duyne and I. Koev, Intensity considerations in liquid core optical fiber Raman spectroscopy, *Appl. Spectrosc.*, 2001, **55**(4), 373–381; (*e*) D. Qi and A. J. Berger, Quantitative concentration measurements of creatinine dissolved in water and urine using Raman spectroscopy and a liquid core optical fiber, *J. Biomed. Opt.*, 2005, **10**(3), 031115; (*f*) Y. Tian, L. Zhang, J. Zuo, Z. Li, S. Gao and G. Lu, Raman sensitivity enhancement for aqueous absorbing sample using Teflon-AF 2400 liquid core optical fibre cell, *Anal. Chim. Acta*, 2007, **581**(1), 154–158; (*g*) D. Qi and A. J. Berger, Quantitative analysis of Raman signal enhancement from aqueous samples in liquid core optical fibers, *Appl. Spectrosc.*, 2004, **58**(10), 1165–1171; (*h*) R. Altkorn, I. Koev, R. P. VanDuyne and M. Litorja, Low-loss liquid-core optical fiber for low-refractive-index liquids: fabrication, characterization, and application in Raman spectroscopy, *Appl. Opt.*, 1997, **36**(34), 8992–8998; (*i*) R. Altkorn, I. Koev and A. Gottlieb, Waveguide capillary cell for low-refractive-index liquids, *Appl. Spectrosc.*, 1997, **51**(10), 1554–1558.

27 T. Frosch, D. Yan and J. Popp, Ultrasensitive Fiber Enhanced UV Resonance Raman Sensing of Drugs, *Anal. Chem.*, 2013, **85**(13), 6264–6271.

28 W. J. Hehre, R. F. Stewart and J. A. Pople, Self-Consistent Molecular-Orbital Methods. I. Use of Gaussian Expansions of Slater-Type Atomic Orbitals, *J. Chem. Phys.*, 1969, **51**(6), 2657–2664.

29 M. J. Frisch, G. W. Trucks, H. B. Schlegel, G. E. Scuseria, M. A. Robb, J. R. Cheeseman, G. Scalmani, V. Barone, B. Mennucci, G. A. Petersson, H. Nakatsuji, M. Caricato, X. Li, H. P. Hratchian, A. F. Izmaylov, J. Bloino, G. Zheng, J. L. Sonnenberg, M. Hada, M. Ehara, K. Toyota, R. Fukuda, J. Hasegawa, M. Ishida, T. Nakajima, Y. Honda, O. Kitao, H. Nakai, T. Vreven, J. A. Montgomery Jr., J. E. Peralta, F. Ogliaro, M. J. Bearpark, J. Heyd, E. N. Brothers, K. N. Kudin, V. N. Staroverov, R. Kobayashi, J. Normand, K. Raghavachari, A. P. Rendell, J. C. Burant, S. S. Iyengar, J. Tomasi, M. Cossi, N. Rega, N. J. Millam, M. Klene, J. E. Knox, J. B. Cross, V. Bakken, C. Adamo, J. Jaramillo, R. Gomperts, R. E. Stratmann, O. Yazyev, A. J. Austin, R. Cammi, C. Pomelli, J. W. Ochterski, R. L. Martin, K. Morokuma, V. G. Zakrzewski, G. A. Voth, P. Salvador, J. J. Dannenberg, S. Dapprich, A. D. Daniels, Ö. Farkas, J. B. Foresman, J. V. Ortiz, J. Cioslowski and D. J. Fox, *Gaussian 09*, Gaussian, Inc., Wallingford, CT, USA, 2009.

30 A. D. Becke, Density-Functional Thermochemistry .2. The Effect of the Perdew-Wang Generalized-Gradient Correlation Correction, *J. Chem. Phys.*, 1992, **97**(12), 9173–9177.

31 P. J. Stephens, F. J. Devlin, C. F. Chabalowski and M. J. Frisch, Ab-Initio Calculation of Vibrational Absorption and Circular-Dichroism Spectra Using Density-Functional Force-Fields, *J. Phys. Chem.*, 1994, **98**(45), 11623–11627.

32 C. Lee, W. Yang and R. G. Parr, Development of the Colle-Salvetti correlation-energy formula into a functional of the electron density, *Phys. Rev. B: Condens. Matter*, 1988, **37**(2), 785–789.

33 (*a*) T. H. Dunning, Gaussian-Basis Sets for Use in Correlated Molecular Calculations .1. The Atoms Boron through Neon and Hydrogen, *J. Chem. Phys.*, 1989, **90**(2), 1007–1023; (*b*) T. H. Dunning, A road map for the calculation of molecular binding energies, *J. Phys. Chem. A*, 2000, **104**(40), 9062–9080.

34 J. A. Pople, H. B. Schlegel, R. Krishnan, D. J. Defrees, J. S. Binkley, M. J. Frisch, R. A. Whiteside, R. F. Hout and W. J. Hehre, Molecular-Orbital Studies of Vibrational Frequencies, *Int. J. Quantum Chem.*, 1981, **20**(S15), 269–278.

35 (*a*) T. Frosch and J. Popp, Relationship between molecular structure and Raman spectra of quinolines, *J. Mol. Struct.*, 2009, **924–926**, 301–308; (*b*) R. Keiner, M. Herrmann, K. Kuesel, J. Popp and T. Frosch, Rapid monitoring of intermediate states and mass balance of nitrogen during denitrification by means of innovative cavity enhanced Raman multi-gas sensing, *Anal. Chim. Acta*, 2015, **864**, 39–47; (*c*) R. Keiner, T. Frosch, T. Massad, S. Trumbore and J. Popp, Enhanced Raman multigas sensing - a novel tool for control and analysis of (13)CO2 labeling experiments in environmental research, *Analyst*, 2014, **139**(16), 3879–3884; (*d*) T. Frosch, R. Keiner, B. Michalzik, B. Fischer and J. Popp, Investigation of gas exchange processes in peat bog ecosystems by means of innovative Raman gas spectroscopy, *Anal. Chem.*, 2013, **85**(3), 1295–1299.

36 (*a*) S. A. Asher, UV resonance Raman studies of molecular structure and dynamics: applications in physical and biophysical chemistry, *Annu. Rev. Phys. Chem.*, 1988, **39**(1), 537–588; (*b*) J. M. Turner, J. N. Gayles and H. M. Turner, Resonance Raman-Spectra of Hemoglobin-a and Hemoglobin-S, *Bull. Am. Phys. Soc.*, 1975, **20**(4), 729–729; (*c*) T. G. Spiro, Resonance Raman spectroscopy. New structure probe for biological chromophores, *Acc. Chem. Res.*, 1974, 7(10), 339–344; (*d*) B. R. Wood, L. Hammer, L. Davis and D. McNaughton, Raman microspectroscopy and imaging provides insights into heme aggregation and denaturation within human erythrocytes, *J. Biomed. Opt.*, 2005, **10**(1), 14005; (*e*) B. R. Wood and D. McNaughton, Raman excitation wavelength investigation of single red blood cells in vivo, *J. Raman Spectrosc.*, 2002, **33**(7), 517–523; (*f*) T. Frosch, T. Meyer, M. Schmitt and J. Popp, Device for Raman Difference Spectroscopy, *Anal. Chem.*, 2007, **79**(16), 6159–6166.

37 (*a*) T. Frosch, M. Schmitt and J. Popp, Raman spectroscopic investigation of the antimalarial agent mefloquine, *Anal. Bioanal. Chem.*, 2007, **387**(5), 1749–1757; (*b*) T. Frosch, M. Schmitt, T. Noll, G. Bringmann, K. Schenzel and J. Popp, Ultrasensitive in situ Tracing of the Alkaloid Dioncophylline A in the Tropical Liana Triphyophyllum peltatum by Applying Deep-UV Resonance Raman Microscopy, *Anal. Chem.*, 2007, **79**(3), 986–993; (*c*) T. Frosch, M. Schmitt, K. Schenzel, J. H. Faber, G. Bringmann, W. Kiefer and J. Popp, In vivo localization and identification of the antiplasmodial alkaloid dioncophylline A in the tropical liana Triphyophyllum peltatum by a combination of fluorescence, near infrared Fourier transform Raman microscopy, and density functional theory calculations, *Biopolymers*, 2006, **82**(4), 295–300; (*d*) T. Frosch and J. Popp, Structural analysis of the antimalarial drug halofantrine by means of Raman spectroscopy and density functional theory calculations, *J. Biomed. Opt.*, 2010, **15**(4), 041516.

38 A. Smith and M. Witty, *Heme, Chlorophyll, and Bilins: Methods and Protocols*, Humana Press, 2001.

39 (*a*) A. Hartung, J. Kobelke, A. Schwuchow, K. Wondraczek, J. Bierlich, J. Popp, T. Frosch and M. A. Schmidt, Double antiresonant hollow core fiber – guidance in the deep ultraviolet by modified tunneling leaky modes, *Opt. Express*, 2014, **22**(16), 19131; (*b*) A. Hartung, J. Kobelke, A. Schwuchow, K. Wondraczek, J. Bierlich, J. Popp, T. Frosch and M. A. Schmidt, Origins of modal loss of antiresonant hollow-core optical fibers in the ultraviolet, *Opt. Express*, 2015, **23**(3), 2557–2565.

40 I. P. Torres, J. Terner, R. N. Pittman, E. Proffitt and K. R. Ward, Measurement of hemoglobin oxygen saturation using Raman microspectroscopy and 532-nm excitation, *J. Appl. Physiol.*, 2008, **104**(6), 1809–1817.

41 T. Orui, H. Yasuda, M. Yamaya, T. Matsui and H. Sasaki, Transient relief of asthma symptoms during jaundice: a possible beneficial role of bilirubin, *Tohoku J. Exp. Med.*, 2003, **199**(3), 193–196.